Towards Optimal Control of Blood Flow in Artificial Hearts

S. Tavoularis[1], A. Sahrapour[1], N. U. Ahmed [2,3], A. Madrane[3], R. Vaillancourt[2,3]

Background: It is well known that high shear stresses and turbulence can cause hemolysis, while alternating and low-level stresses that are often encountered in recirculation and stagnation regions may contribute to platelet activation and thrombus formation. The objective of this study is to apply the mathematical theory of optimal control to the driving system of artificial hearts in order to minimize flow-related potential problems.

Methods: Blood flow in large vessels may be approximated by unsteady, incompressible flow of a Newtonian fluid, which is described by the Navier-Stokes (momentum) and continuity equations. An optimization problem is set up such that it selects the optimal variation of flow velocity at a wall (simulating the motion of a pusher plate or a diaphragm) in order to minimize a criterion (cost functional) as well as satisfy certain imposed constraints. A tentative cost functional contains the mean squared shear stress and the mean squared vorticity in the entire flow domain and the mean squared velocity on the control boundary. Constraints include matching of the natural flow rate variation during a cycle and maintaining a zero net displacement of all points on the control boundary during a cycle. The imposition of optimality results in an adjoint set of equations, which have to be satisfied simultaneously with the equations of motion. The solution of all equations is obtained by an iterative numerical algorithm.

Results: Examples of the application of this method are presented for a prototype artificial heart, which is an idealized model of sac-type ventricular assist devices with alternately opening and closing inlet and outlet ports. It is demonstrated that application of optimal control results in flows with reduced stresses and recirculation.

Conclusion: The general conclusion of this study is that optimal control methods are a promising approach for optimizing the design and operation of artificial hearts and, by inference, other medical devices involving the flow of fluids.

(CVE. 2003; 8 (1/2): 20-31)

Key words: artificial heart, diaphragm, optimal control, blood flow

1. Introduction

Since their conceptualization in the 1960s, artificial hearts of different designs have been under continuous development. The operation of such devices is hampered by potentially serious hemodynamic problems, notably hemolysis and thrombogenesis, which have been correlated with elevated turbulent shear stresses and recirculation or stagnation in the device. High turbulence activity can cause lysis of red cells and platelet activation, possibly leading to clot formation and thrombosis (Stein and Sabbah, 1974; Goldsmith and Skalak, 1975; Blackshear and Blackshear, 1987). The severity of shear-related damage to blood constituents is highly influenced by both the magnitude and the duration of the shear stress (Tiederman et al., 1986). In addition to high shear rates, slow flows in separated regions and near stagnation points may also contribute to thrombus formation (see, e.g., Galanga and Lloyd, 1981).

The shape and size of artificial hearts are usually the results of empirical design, within constraints dictated by physiological considerations, power source limitations, biocompatibility of materials and ease in surgical implantation. Following the traditional approach used in the development of many other technological systems, improvements in artificial heart design and mode of operation have been based on a judicious combination of intuition, skill and trial-and-error testing of competing alternative solutions (e.g. Mussivand et al., 1999). Nevertheless, it seems plausible that geometrical dimensions and shapes may be optimized following a systematic analytical approach, although the optimal overall geometrical design, if such exists, is rather unlikely to be provided by an analytical

From the [1]Department of Mechanical Engineering; [2]School of Information Technology and Engineering; [3]Department of Mathematics and Statistics, University of Ottawa, Ottawa, Ontario, Canada

Reprints requests to: Prof. Stavros Tavoularis, Department of Mechanical Engineering, University of Ottawa, Ottawa, Ontario, Canada K1N 6N5, E-mail: tav@eng.uottawa.ca

algorithm. Even more plausible is the hypothesis that, given a particular heart design, one may minimize the probability of blood damage and thrombus formation by controlling the flow generating system.

In view of the above comments, it seems a worthwhile endeavour to attempt to optimize blood flow in artificial hearts by the application of formal optimal control theory, which has already been developed and applied to a variety of systems, including systems involving fluid flows. Following several decades of exploration, the mathematical foundations of optimal control of viscous flows are now reasonably well understood (Sritharan, 1998) and many researchers are applying this technique to the solution of diverse problems of practical interest. Examples include the reduction of turbulent shear stresses on immersed objects, the control of combustion and chemical reactions, and the prediction of oceanic and atmospheric flows (e.g. Abergel and Temam, 1990; Gunzburger et al., 1992).

The objective of the present research is to demonstrate that optimal control theory is capable of minimizing flow related problems in artificial hearts, and, by implication, in other artificial organs and clinical devices. The problems involved in this process are highly complex and require expertise in different areas, including fluid dynamics, physiology, solid mechanics, engineering design, mathematics, optimal control theory and numerical methods. In order to develop this method to a point that it may be used as a practical design tool for artificial hearts, one would have to resolve many different issues, for which the existing literature provides little support. First, one would have to develop a sound and accurate mathematical model of an operating artificial heart connected to the cardiovascular system of the patient. Then, one would have to determine a mathematical function that may serve as a criterion for minimizing hemodynamic problems. An important step is to formulate a mathematical problem that admits an optimal solution and to prove that such a solution exists. And, finally, one has to develop a numerical algorithm that can solve the mathematical problem and produce the optimal solution. It goes without saying that any results produced by this approach would have to be scrutinized for mathematical, numerical, physical and physiological soundness and, to the greatest possible extent, compared to experimental, *in vitro* and *in vivo*, realizations.

The present work is still in a stage of development and the results presented here are quite tentative and preliminary. In order to proceed with the mathematical formulation, we have decided to adopt a simplified performance criterion that is possible to implement following existing practices. As a representative example for the application of the technique we have selected a relatively crude model of a typical sac-type ventricular assist device. Furthermore, we have made a number of other simplifications, trying to maintain a balance between a realistic representation of the actual problem and convenience in the implementation of the method. Earlier variations of this work were presented by Sahrapour et al. (1993 and 1994), while details concerning earlier formulations and the numerical algorithm have been outlined by Sahrapour (1995).

2. Methods

In this section, we will first summarize, as a background, the essential components of an optimal control problem. Then, we will briefly discuss the possible choices of components for the problem of artificial heart control and will identify the choices made for the present work, leading to a set of mathematical conditions that have to be satisfied. Finally, we will outline the numerical solution algorithm that will be applied.

2.1 Components of a General Optimal Control Problem

In any formulation of an optimal control problem dealing with fluid flow, one may identify the following typical components.

- One or more *state variables*, which are the parameters that describe the motion of the fluid system. The variation of the state variables is subject to physical constraints, such as the conservation of mass, the momentum principle and the energy principle. These constraints are expressed in the form of mathematical equations (*equations of motion*), containing the state variables as unknowns. Additional relationships may be necessary to satisfy specific requirements of the solution, as, for example, the specification of a flow rate variation.
- One or more *control variables*, which are parameters whose values can be prescribed and set by external means and whose variation determines the values of the state variables.
- A *performance criterion*, by which one may evaluate the desirability of each combination of state variables and control variables. This criterion is expressed mathematically as a function (*performance, objective or cost functional*) of the control and state variables.
- The *conditions of optimality*, which include the equations of motion and other equations or inequalities, as dictated by the mathematical analysis of the optimization problem.
- An *optimization algorithm*, which is capable of computing the set of control variables (*optimal control*) that minimizes (or, in some cases, maximizes) the performance functional. The same algorithm computes the corresponding set of state variables, which, at all times, satisfy the relevant equations of motion and the other conditions of optimality.

2.2 A Simplified Model of an Artificial Heart and its Operation

Whole blood, as a suspension, is a non-Newtonian fluid, which means that its internal stresses cannot, in general, be represented as linear functions of the rate of deformation (Fung, 1993). However, at the high shear rates occurring

near the walls of the heart and the pulmonary and systemic arteries and veins, whole blood can be modeled as a Newtonian fluid with a constant coefficient of viscosity (Pedley, 1980; Fung, 1990; Fung, 1993). For simplicity, blood flow in artificial hearts will be considered as Newtonian, although the incorporation of a non-Newtonian model into the formulation appears also to be possible.

Among the different designs of artificial hearts, we have selected as representative a sac-type ventricular assist device, for which geometrical and hemodynamic information is readily available (Jin and Clark, 1993). To avoid excessive complications in the numerical computation, we have simplified the shape of this device and also made the following, rather drastic, approximations.

- Instead of a heart connected to a patient and, thus, coupled to the entire cardiovascular system, we have considered an isolated device that is connected, through its inlet and outlet ports, to chambers of infinite size, containing the same fluid at a uniform pressure.
- The numerical simulations of flows with moving boundaries and of fluid-structure interaction remain extremely challenging problems of computational fluid dynamics. For this preliminary study, we have approximated the moving surfaces in the device as follows.
  - The elastic diaphragm has been replaced by a fixed plane, through which the normal flow velocity may be prescribed (see below). This velocity is allowed to vary across the plane and simulates the velocity imposed upon the fluid by the moving diaphragm. This approximation appears to be reasonable as long as the displacement of the diaphragm is small.
  - The tilting-disk-type valves at the inlet and outlet ports were replaced also by fixed planes. Each port would be either entirely open or entirely closed to the flow, depending on whether the flow cycle was in its diastolic or systolic phase.
- A flow rate variation through the device during a cycle of operation was prescribed to match the flow rate waveform observed by Jin and Clark (1993). Thus, the pulsatile nature of blood flow through the device was approximated by simple means.

A realistic control variable for several popular designs of artificial hearts and ventricular assist devices would be the oscillatory motion of a pusher plate or diaphragm. In the sac-type device of Jin and Clark (1993), the diaphragm was driven by pressurized air contained in an adjacent chamber and supplied by a pneumatic driver with nominally square-wave outputs for both positive and suction pressures. The accurate representation of such a complex system is beyond our current capabilities and resources (see also Ahmed, 1995). For mathematical and numerical simplicity, we model the motion of the diaphragm by a time dependent boundary velocity distribution over a plane that simulates the boundary occupied by the diaphragm at its equilibrium position. Thus, the control variable is the variation of this boundary velocity over one cycle of operation, assuming that steady state has been achieved following many cycles of operation.

Now, we proceed with the formulation of the equations of motion. First of all, we denote by Ω the domain occupied by the fluid inside the device, which is assumed to be a three-dimensional open bounded set in $\mathbf{R}^3$, whose boundary is denoted by $\Gamma = \Gamma_m \cup \Gamma_f \cup \Gamma_i \cup \Gamma_o$. Γ_m is the part of the boundary over which the velocity is prescribed as the control variable; Γ_f is a rigid wall over which the velocity vanishes; Γ_i is the inlet boundary, which is open during part of the cycle (diastole) and closed during the remainder of the cycle (systole); and Γ_o is the outlet boundary, open during systole and closed during diastole.

A length scale and a velocity (or time) scale are required in order to present the equations in dimensionless form. The diameter of the diaphragm, d_s, is an appropriate length scale. The time-averaged volume flow rate through the device, Q_s, is a parameter that must be specified, as required for its proper operation. Then, one may define a velocity scale as $u_s = Q_s/(\pi_s^2/4)$. The corresponding time scale is $t_s=d_s/u_s$. All geometric and kinematic parameters will be non-dimensionalized by the above scales. The pressure will be made dimensionless by twice the dynamic pressure, ρu_s^2, where ρ is the fluid density. A dimensionless parameter of dynamic importance is the Reynolds number $Re = \rho u_s d_s/\mu$, where μ is the viscosity of the fluid, assumed to be constant. The operation of the device will be assumed to be periodic with a dimensionless period equal to T, out of which a portion T_1 will be occupied by systole, while the remainder $T - T_1$ by diastole.

A sufficient set of equations describing the time dependent motion of an incompressible Newtonian fluid with constant properties consists of the momentum (Navier-Stokes; vector) and the continuity (scalar) equations, as follows (boldface characters represent vectors)

$$
\begin{cases}
\dfrac{\partial \mathbf{u}}{\partial t} + (\mathbf{u}\cdot\nabla)\mathbf{u} - \dfrac{1}{Re}\nabla^2\mathbf{u} + \nabla p = \mathbf{f} \quad \text{in } \Omega \times (0,T], \\
\nabla\cdot\mathbf{u} = 0 \quad \text{in } \Omega, \\
\mathbf{u}|_{t=0} = \mathbf{u}(\mathbf{x},0) = 0 \quad \text{in } \Omega, \qquad \mathbf{u}|_{\Gamma_m} = \mathbf{g}(\mathbf{x},t). \qquad \mathbf{u}|_{\Gamma_f} = 0, \\
\mathbf{u}|_{\Gamma_i} = 0, \qquad \left.\dfrac{\partial \mathbf{u}}{\partial \mathbf{n}}\right|_{\Gamma_o} = 0, \qquad 0 < t \le T_1, \\
\left.\dfrac{\partial \mathbf{u}}{\partial \mathbf{n}}\right|_{\Gamma_i} = 0, \qquad \mathbf{u}|_{\Gamma_o} = 0, \qquad T_1 < t \le T,
\end{cases}
\tag{1}
$$

where $\mathbf{x} = (x_1,x_2,x_3)$ denotes the dimensionless position vector; t the dimensionless time; $\mathbf{u} = (u_1,u_2,u_3)$ the dimensionless velocity vector; $\mathbf{n}$ the dimensionless unit vector normal to a boundary; $\mathbf{f} = (f_1, f_2, f_3)$ the dimensionless body force (weight; a vector); and $\mathbf{g}(\mathbf{x},\mathbf{t})$ the dimensionless velocity vector on the boundary representing the diaphragm.

The primary state variables in the present problem are the velocity and pressure variations as functions of position and time. Once these variables have been computed, other parameters of interest, such as wall- and in-flow stresses, vorticity and residence time of the fluid in the device may be easily calculated.

A comment concerning the relevance of the above equations is in order. Operating artificial hearts are likely to generate turbulence, at least over part of the cycle. The Navier-Stokes and continuity equations listed above apply equally well to laminar and turbulent flows. However, the

accurate simulation of turbulent flows remains a very challenging problem. In particular, the simulation of transition to turbulence in a time-dependent flow at moderate Reynolds numbers has not yet been achieved in a satisfactory manner. A promising approach for resolving this issue is Large Eddy Simulation (LES), in association with a dynamic eddy viscosity model (Lesieur and Métais, 1996; Meneveau and Katz 2000). In the present analysis, only laminar flows will be considered. Although, in general, laminar flows are easier to compute than turbulent ones, their numerical solution is known not to converge as the Reynolds number increases, especially during rapid deceleration of the flow, which enhances instability and transition to turbulence.

2.3 The Performance Criterion

Although a literature survey has identified certain types of hemodynamic problems that the designer of artificial hearts has to take into consideration, it has not produced a clear criterion for optimal design. The following discussion, should, therefore, be regarded as tentative and of pioneering nature.

As mentioned in the introduction, blood may be adversely affected by large shear stresses. For Newtonian fluids, the viscous shear stress is proportional to the velocity gradient $\nabla\mathbf{u}$, whose magnitude must therefore be controlled. Mathematically, this is easier to achieve in the mean square sense, over the entire domain Ω and time interval $I = [0,T]$. This introduces the quantity

$$\int_I\int_\Omega |\nabla\mathbf{u}(\mathbf{x},t)|^2\, d\mathbf{x}\, dt \tag{2}$$

as a possible term in the cost functional. It must be emphasized, however, that a relatively low level of mean square stress does not necessarily preclude the appearance of large stresses concentrated locally or over a short time. Furthermore, a substantial mean square stress that is accompanied by instantaneous stresses that never exceed the threshold for hemolysis and thrombogenesis may not be a problem. Another limitation of this parameter is that it cannot take into account turbulent stresses, which can be several orders of magnitude larger than the local viscous stresses.

Another well-known flow-related problem is caused by the recirculation and stagnation of blood within the device, which encourages the formation of clots. It is not clear how to express this phenomenon mathematically. Perhaps minimizing the mean square residence time of blood inside the device over several cycles would be an appropriate strategy. For mathematical simplicity, we chose to represent this aspect by the mean square vorticity

$$\int_I\int_\Omega |\nabla\times\mathbf{u}(\mathbf{x},t)|^2\, d\mathbf{x}\, dt. \tag{3}$$

Low vorticity is equivalent to low circulation in the device and likely to signify a lower chance for flow separation and recirculation. Once more, the relevance of this criterion remains to be verified.

Following common practice in optimal control analyses, one may also try to minimize the total energy spent on the system, which, in the present case, is represented by the kinetic energy of the flow at the control boundary $|\mathbf{g}(\mathbf{x},t)|^2$.

Then, a tentative cost functional may be introduced as a weighted sum of the L^2 norms of the appropriate quantities in $\Omega\times I$, as follows:

$$\begin{aligned} J(\mathbf{u},\mathbf{g}) &= \frac{\alpha_s}{2}\int_I\int_\Omega |\nabla\mathbf{u}(\mathbf{x},t)|^2\, d\mathbf{x}\, dt + \frac{\alpha_v}{2}\int_I\int_\Omega |\nabla\times\mathbf{u}(\mathbf{x},t)|^2\, d\mathbf{x}\, dt \\ &\quad + \frac{\alpha_e}{2}\int_I\int_{\Gamma_m} |\mathbf{g}(\mathbf{x},t)|^2\, ds\, dt, \end{aligned} \tag{4}$$

where $\mathbf{u}$ is the solution of system (1) corresponding to control $\mathbf{g}$ and the weights α_v, α_s *and* α_e may be adjusted to reflect the emphasis assigned to each term of the cost functional.

Besides the above requirements, the solution must satisfy additional constraints. An important one is to match a prescribed average flow rate during each cycle, as required for the supply of adequate blood to the patient. We will go a step further and require that the instantaneous flow rate through the device be matched; in other words, we will prescribe the variation of flow rate (desired flow rate, nondimensionalized by Q_s), $Q^d(t)$, measured by Jin and Clark (1993) and force the solution to match it, namely require that

$$\int_I |Q(t) - Q^d(t)|^2\, dt = 0. \tag{5}$$

where $Q(t) = \int_{\Gamma_m} \mathbf{u}(x,t)ds.$

The motion of the elastic diaphragm that drives the blood has been modelled in the present approximation as a boundary velocity of the fluid over the boundary Γ_m. In order to introduce some realism into this approximation, we will impose the constraint that the net dimensionless displacement of all fluid particles on Γ_m should be zero over one cycle:

$$\int_{\Gamma_m}\left|\int_I \mathbf{u}\, dt\right|^2 ds = 0, \tag{6}$$

which corresponds to the return of the diaphragm to its equilibrium position at the end of each cycle.

The above constraints may be satisfied using the Lagrange multiplier formalism. We introduce the Lagrangian function

$$\begin{aligned} \mathcal{L}(\mathbf{u},\mathbf{g},\lambda,\beta,\mathbf{z}) &= J(\mathbf{u},\mathbf{g}) + \frac{1}{2}\lambda\int_I |Q(t) - Q^d(t)|^2\, dt + \frac{1}{2}\beta\int_{\Gamma_m}\left|\int_I \mathbf{u}\, dt\right|^2 ds \\ &\quad + \int_I\int_\Omega \mathbf{z}\cdot\left[\frac{\partial\mathbf{u}}{\partial t} + (\mathbf{u}\cdot\nabla)\mathbf{u} - \frac{1}{Re}\nabla^2\mathbf{u} + \nabla p - \mathbf{f}\right] d\mathbf{x}\, dt. \end{aligned} \tag{7}$$

where λ, β and **z** are the Lagrange multipliers and the last term has been added to account for the equations of motion. The resulting conditions of optimality will be discussed in the following section.

2.4 The Mathematical Conditions for Optimality

Our objective is to determine a control variable $\mathbf{g}(\mathbf{x},t) \in U_{ad}$ (where the set of admissible controls, U_{ad}, is a closed convex set in $L^2((0,T) \times \Gamma_m)$), which would produce the optimal state that minimizes the cost functional in equation (4) as well as satisfies the constraints (1), (5) and (6). The pair ($\mathbf{g}^0$, $\mathbf{u}^0$) satisfying these requirements is called the *optimal pair*.

Setting to zero the first variation of $\mathcal{L}$ with respect to the Lagrange multipliers **z**, λ and β yields the constraint equations (1), (5) and (6), respectively. Setting to zero the first variations with respect to the state velocity **u** yields the adjoint system of equations (see equation (9) below). Finally, setting to zero the first variation with respect to the control **g** gives the optimality condition (10) below.

Details of the mathematical derivations are omitted here. The existence of an optimal control, namely of at least one element $\mathbf{g}^0 \in U_{ad}$ such that $J(\mathbf{u},\mathbf{g}^0) \le J(\mathbf{u},\mathbf{g})$, for all $\mathbf{g} \in U_{ad}$, has been proved by Ahmed (1992) (with a slightly different cost functional and without constraints (5) and (6)). However, the question of uniqueness of optimal control has not yet been resolved. In general, because the mapping $\mathbf{g} \to \mathbf{u}_g$ is nonlinear, $J(\mathbf{u},\mathbf{g})$ is nonconvex and uniqueness cannot be guaranteed (see Abergel and Temam, 1990).

Consider the system of equations (1). Assume that the integrand, l, of the cost functional in (4) is once continuously Gâteaux differentiable and denote the Gâteaux derivatives of l with respect to the state **u** and the control **g** by $\mathbf{G}^1$ and $\mathbf{G}^2$, respectively. Then, in order that the pair ($\mathbf{g}^0$, $\mathbf{u}^0$) be the optimal pair, it is necessary that there exists a $\mathbf{z}^0(\mathbf{x},t)$ such that the triplet ($\mathbf{g}^0$,$\mathbf{u}^0$,$\mathbf{z}^0$) satisfies the following equations (8) and (9) and inequality (10):

$$\begin{cases} \dfrac{\partial \mathbf{u}^0}{\partial t} + (\mathbf{u}^0 \cdot \nabla)\mathbf{u}^0 - \dfrac{1}{Re}\nabla^2 \mathbf{u}^0 + \nabla p^0 = \mathbf{f} \quad \text{in } \Omega \times (0,T], \\ \nabla \cdot \mathbf{u}^0 = 0 \quad \text{in } \Omega, \\ \mathbf{u}^0|_{t=0} = \mathbf{u}^0(\mathbf{x},0) = 0 \quad \text{in } \Omega, \qquad \mathbf{u}^0|_{\Gamma_m} = \mathbf{g}^0(\mathbf{x},t), \qquad \mathbf{u}^0|_{\Gamma_f} = 0, \\ \mathbf{u}^0|_{\Gamma_i} = 0, \qquad \left.\dfrac{\partial \mathbf{u}^0}{\partial \mathbf{n}}\right|_{\Gamma_o} = 0, \qquad 0 < t \le T_1, \\ \left.\dfrac{\partial \mathbf{u}^0}{\partial \mathbf{n}}\right|_{\Gamma_i} = 0, \qquad \mathbf{u}^0|_{\Gamma_o} = 0, \qquad T_1 < t \le T; \end{cases} \tag{8}$$

$$\begin{cases} -\dfrac{\partial \mathbf{z}^0}{\partial t} - (\mathbf{u} \cdot \nabla)\mathbf{z}^0 + (\nabla \mathbf{u})^T \mathbf{z}^0 - \dfrac{1}{Re}\nabla^2 \mathbf{z}^0 + \nabla q_z^0 = \mathbf{G}^1(\mathbf{u}^0, \mathbf{g}^0) \qquad \text{in } \Omega \times (0,T], \\ \nabla \cdot \mathbf{z}^0 = 0 \quad \text{in } \Omega, \\ \mathbf{z}^0|_{t=T} = \mathbf{z}^0(\mathbf{x},T) = 0 \quad \text{in } \Omega, \qquad \mathbf{z}^0|_{\Gamma_m} = 0, \qquad \mathbf{z}^0|_{\Gamma_f} = 0, \\ \mathbf{z}^0|_{\Gamma_i} = \lambda(Q^0 - Q^d), \qquad \mathbf{z}^0|_{\Gamma_o} = 0, \qquad 0 < t \le T_1, \\ \mathbf{z}^0|_{\Gamma_i} = 0, \qquad \mathbf{z}^0|_{\Gamma_o} = \lambda(Q^0 - Q^d), \qquad T_1 < t \le T; \end{cases} \tag{9}$$

and

$$\begin{aligned} &< \mathcal{L}'(\mathbf{u},\mathbf{g}^0,\lambda,\beta,\mathbf{z}), \mathbf{g} - \mathbf{g}^0 > \\ &= \int_I \int_{\Gamma_m} \left[-\frac{1}{Re}(\mathbf{n} \cdot \nabla)\mathbf{z}^0 + \mathbf{G}^2(\mathbf{u}^0, \mathbf{g}^0) + q_z \mathbf{n} \right] \cdot (\mathbf{g} - \mathbf{g}^0)\, ds\, dt \\ &\ge 0 \qquad \forall \mathbf{v} \in U_{ad}. \end{aligned} \tag{10}$$

The system of equations (9) represents the adjoint equations along the optimal flow $\mathbf{u}^0$. The variables **z** and q_z are called the adjoint state and adjoint pressure, respectively. It should be noted that the definition of the initial condition for the adjoint state **z** is at time $t=T$, in contrast to the definition of the initial condition (t=0) in the Navier--Stokes equations. This is an important feature of the adjoint field.

2.5 The Numerical Solution Procedure

In order to compute the optimal control-state pair ($\mathbf{g}^0$,$\mathbf{u}^0$), we used a gradient type algorithm based on the necessary conditions of optimality stated in equations (8)-(10). This approach uses the gradient of the Lagrangian function $\mathcal{L}(\mathbf{u}^0, \mathbf{g}^0, \lambda, \beta, \mathbf{z}^0)$ with respect to the control, which leads to an iterative computation of the optimal control. This iterative algorithm is summarized in the following steps.

Step 1: Specify values for **g**, λ and β for the first iteration.

Step 2: At the n-th step, with $\mathbf{g}_n$ specified, the system of equations (8) is solved for ($\mathbf{u}_n$, p_n) by forward marching in time.

Step 3: With ($\mathbf{u}_n$, $\mathbf{g}_n$) specified, equation (9) is solved for the adjoint pair ($\mathbf{z}_n$, q_n) by backward marching in time.

Step 4: With ($\mathbf{g}_n$, $\mathbf{u}_n$, $\mathbf{z}_n$) specified, the following gradients are computed at each discrete time step:

$$\mathcal{L}'_g(\mathbf{u}_n, \mathbf{g}_n, \lambda_n, \beta_n, \mathbf{z}_n) = -\frac{1}{Re}(\mathbf{n} \cdot \nabla)\mathbf{z}_n + \mathbf{G}^2(\mathbf{u}_n, \mathbf{g}_n) + q_z \mathbf{n} \quad \text{on } \Gamma_m, \tag{11}$$

$$\mathcal{L}'_\lambda(\mathbf{u}_n, \mathbf{g}_n, \lambda_n, \beta_n, \mathbf{z}_n) = \frac{1}{2}\int_I |Q_n(t) - Q^d(t)|^2\, dt, \tag{12}$$

$$\mathcal{L}'_\beta(\mathbf{u}_n, \mathbf{g}_n, \lambda_n, \beta_n, \mathbf{z}_n) = \frac{1}{2}\int_{\Gamma_m} \left| \int_I \mathbf{u}_n(x,t)\, dt \right|^2 ds. \tag{13}$$

Step 5: New $\mathbf{g}_{n+1}(t)$, λ_{n+1} and β_{n+1} are calculated from the following equations

$$\mathbf{g}_{n+1} = \mathbf{g}_n + \epsilon_1 \mathcal{L}'_g(\mathbf{u}_n, \mathbf{g}_n, \lambda_n, \beta_n, \mathbf{z}_n), \tag{14}$$

$$\lambda_{n+1} = \lambda_n + \epsilon_2 \mathcal{L}'_\lambda(\mathbf{u}_n, \mathbf{g}_n, \lambda_n, \beta_n, \mathbf{z}_n), \tag{15}$$

$$\beta_{n+1} = \beta_n + \epsilon_3 \mathcal{L}'_\beta(\mathbf{u}_n, \mathbf{g}_n, \lambda_n, \beta_n, \mathbf{z}_n), \tag{16}$$

for a suitable choice of the (positive) descent parameters ϵ_1, ϵ_2 and ϵ_3.

Step 6: The quantity $||\mathbf{g}_{n+1} - \mathbf{g}_n||$ is computed using the L^2 norm. If

$$\|\mathbf{g}_{n+1} - \mathbf{g}_n\| + |\lambda_{n+1} - \lambda_n| + |\beta_{n+1} - \beta_n| \le \gamma,$$

for $\gamma > 0$ sufficiently small, the computation is stopped and $\mathbf{g}_{n+1}(t)$ and the corresponding $\mathbf{u}_{n+1}(t)$ are taken as the approximate optimal control and the optimal state, respectively. Otherwise, the

steps 2 through 6 are repeated with $\mathbf{g}_{n+1}(t)$ as the new control.

In step 3 of the above algorithm, the right-hand side, $\mathbf{G}^1$, of the first equation in (9) is found by computing the Gâteaux derivative of the cost functional with respect to the state variable **u**. Then, the Gâteaux derivative, $\mathbf{G}^2$, of the cost functional with respect to the control variable **g** is computed, which in turn is used in (11) together with the adjoint state **z** to find $\mathcal{L}'_g$.

The system of the equations of motion and adjoint equations was solved by the finite element method. The penalty function formulation of the Navier-Stokes equations with **u** and p as unknowns was used (see Girault and Raviart, 1986). Zero initial conditions for the Navier-Stokes equations were used to start the first control iteration. For each subsequent control iteration, the flow solution from the previous iteration was used as the initial condition for the Navier-Stokes equations at that iteration. In view of the nonlinearity of the Navier-Stokes equations, the convergence of the flow solution was checked at each time step by evaluating the relative error. After solving the Navier-Stokes equations, the adjoint equations were solved for all time steps. The simulation was performed using a finite element code developed for this purpose, which uses the Galerkin approach in discretizing both the Navier-Stokes and the adjoint equations. The discretized finite element equations were solved using a slightly modified version of an out-of-core equation solver (see Hasbani and Engelman, 1979). All computations were carried out on a shared IBM AIX 3.2 workstation.

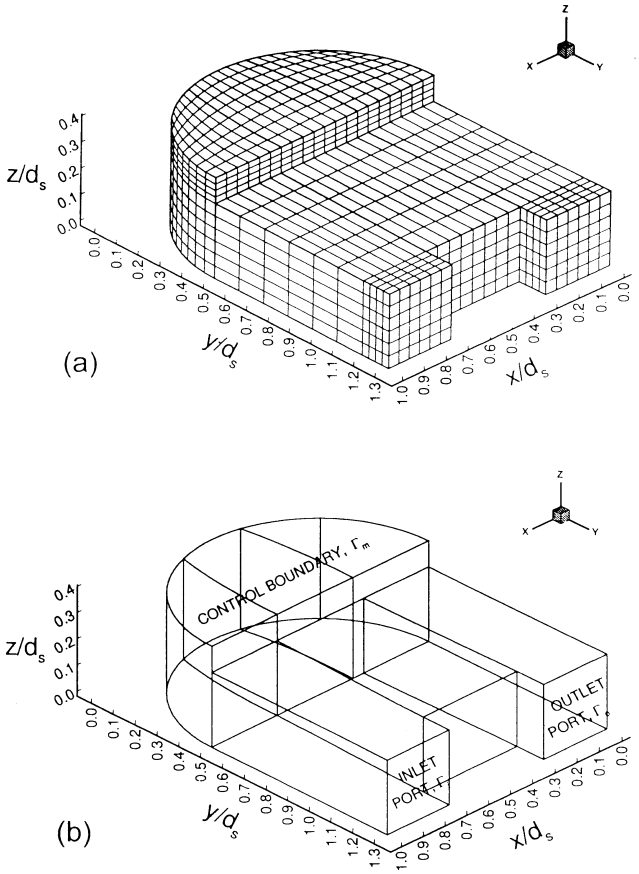

Fig. 1: a) Sketch of the simplified artificial heart and the computational mesh; b) Definitions of the control, inlet and outlet boundaries.

3. Results

The following example is meant to illustrate the plausibility of the optimization algorithm discussed in the previous section. The physical domain used in this example is an idealization of a moving-diaphragm type artificial heart with outlet and inlet ports and a crude approximation of the sac-type ventricular assist device studied by Jin and Clark (1993).

First, let us summarize the flow conditions in the Jin and Clark (1993) experiments. The diameter of their diaphragm was d_s=0.065 *m*. From the given pulsation rate of 70 pulses per minute, the period of the pulsatile cycle of operation of the device was calculated as 0.857 *s*, with 0.300 *s* occupied by the systole and 0.557 *s* occupied by the diastole. The corresponding angular frequency of pulsation was ω =5.39 *rad/s*. Jin and Clark provided the average flow rate produced by their device as 4.05 *l/min*. This results in an average velocity (over the full cycle) of 0.020 *m/s* through the device. Assuming blood to be a Newtonian fluid with a kinematic viscosity of $\nu = 3.5 \times 10^{-6}\ m^2/s$, one may estimate the average Reynolds number as Re =378. The Womersley number based on the diaphragm radius was $\alpha = (d_s/2)/(\nu/\omega)^{1/2} = 40.3$.

The physical domain used in the present study and the finite element mesh are shown in Figure 1. The domain was divided into 326 27-node elements (mid-side nodes are also shown connected in the figure). The flow was generated by a boundary velocity applied on the control boundary Γ_m, which simulates the motion of the diaphragm. The period of pulsation and the systolic/diastolic times were taken as equal to the Jin and Clark values. Thus, the dimensionless period was T=0.270 and the dimensionless systolic time was T_1=0.094. The period was divided into 20 equal time intervals, used as time steps. The Womersley number in the present simulations was the same as the one in the Jin and Clark experiments. With the use of the present relatively crude mesh and time step, we could not attain convergence of the solution for Re > 277, so results are presented for the Re = 277 case. It is speculated that refinements in the mesh size and time step would permit the computation of flow at the Re achieved by Jin and Clark. The dimensionless time-dependent desired flow rate, $Q^d(t)$, was assumed to have the variation shown in Figure 2, which was meant to approximate the waveform measured by Jin and Clark. Obviously,

$$\int_0^{T_1} |Q^d(t)|\,dt = \int_{T_1}^{T} |Q^d(t)|\,dt = 1. \tag{17}$$

The problem was solved for one cycle of operation. During systole the outlet port was open and the inlet port was closed, while during diastole the inlet port was open

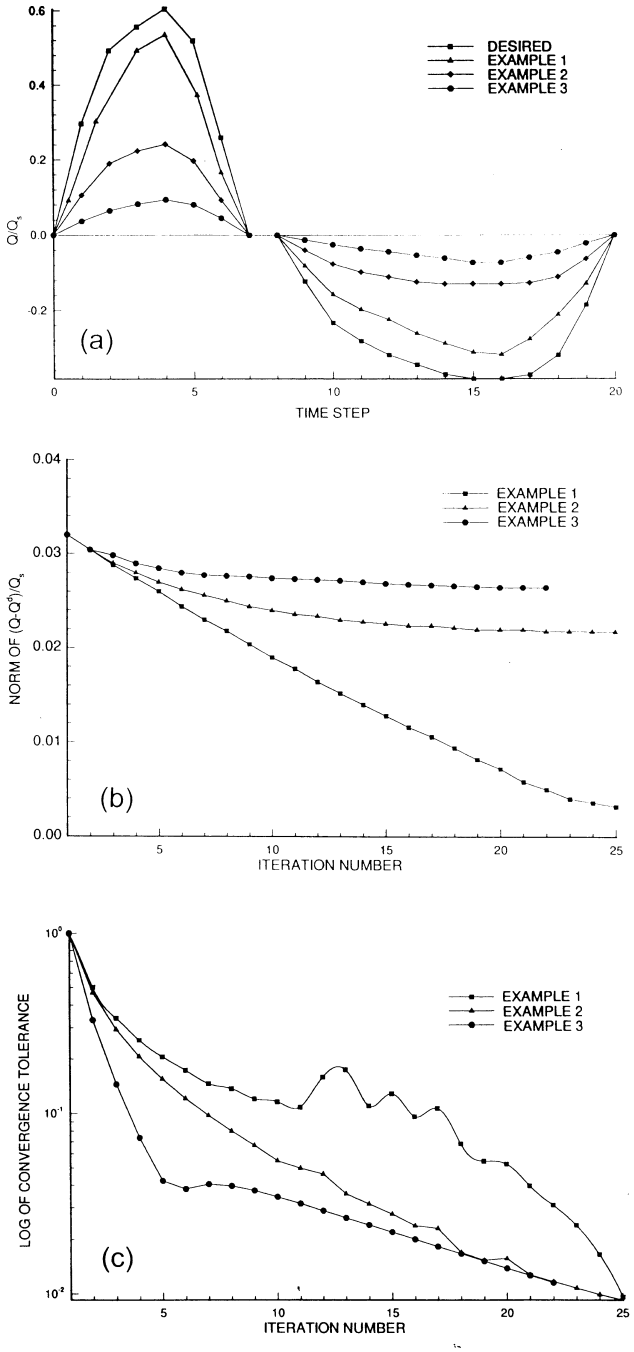

Fig. 2: a) Desired and computed flow rates in examples 1-3; b) variation of the dimensionless norm of the difference between the desired and computed flow rates for the three examples; and c) convergence history for the three examples.

while the outlet port was closed. The no-slip boundary condition was applied to closed ports, while the shear-free boundary condition was applied to open ports.

Three examples of the application of the above algorithm are presented here; example 2 is a variation of example 3 and it is not discussed in detail. In fact, these results correspond to a formulation that is slightly different from the one presented above; the constraint of matching the desired flow rate (equation (5)) was not included in equation (7), but it was incorporated into the cost functional (equation (4)), after being multiplied by the weight $\alpha_d/2$.

In example 1, all weights in the cost functional were set equal to zero, except for the weight for the desired flow rate, which was set as $\alpha_d = 1.000$. Therefore, in example 1, no attempt was made to optimize the flow and the only requirement was to maintain the desired flow rate through the cycle; the constraint of equation (6) was also ignored. In example 2, the weights for the terms representing mean square stress and mean square vorticity were given non-zero values ($\alpha_s = \alpha_v = 0.001$, $\alpha_e = 0.000$, $\alpha_d = 1.000$, $\lambda = 0$, $\beta = 0$), thus enforcing a solution that minimizes these parameters. Example 3 assigned even larger positive values to α_s and α_v ($\alpha_s = \alpha_v = 0.004$, α_e =0.000, α_d =1.000, $\lambda = 0$, $\beta = 0$), in order to increase the importance of low-vorticity and low-stress requirements, compared to the requirement of achieving the desired flow rate.

The variations of the flow rates achieved in the three examples are compared to the specified desired flow rate in Figure 2a. It may be seen that the differences between the desired and achieved flow rates were relatively small (less than 12%) for example 1, but they increased (up to 50%) for example 2 and even more (up to 75%) for example 3. In future computations we hope to eliminate such differences by satisfying the desired flow rate constraint via the current Lagrange multiplier formulation. A similar observation may be made in Figure 2b, showing the convergence history of the norm of $Q–Q^d$. In example 1, this norm approached zero, while, in examples 2 and 3, it approached positive asymptotes. Figure 2c shows the convergence rate of the solution vs. the number of iterations and demonstrates convergence for all three examples; it is noted that, for the same mesh and time step, the solution diverged at higher Reynolds numbers.

Typical velocity vector plots and streamlines for examples 1 and 3 are shown in Figures 3 to 6. The systolic peak (t/T=0.20) and diastolic peak (t/T=0.76) times were selected as representative. It is clear that the fluid crosses at high speed the port that is open, while it essentially stagnates in a large region near the closed port. At systolic peak (Figures 3 and 4), the corresponding plots for the two examples are not very different; this is not surprising, because the flow during systole is accelerating and it is unlikely to develop much recirculation. In contrast, at diastolic peak (Figures 5 and 6), the corresponding plots for examples 1 and 2 show significant differences. The streamline plots for example 1 (Figures 6a-c) illustrate the formation of a 3-D recirculation pattern, indicating that some of the fluid circulates around the "dead zone" before it exits through the boundary representing the diaphragm. For example 3 (Figures 6d-f), however, this recirculating streamline has disappeared. Furthermore, at diastolic peak, the stagnation region near the closed port is visibly larger for example 1 than for example 3. The differences in flow patterns for the two examples are due to differences in the control variable, namely the boundary velocity at the boundary Γ_m.

The latter differences are illustrated in Figure 7, which plots the evolutions of the boundary velocity across Γ_m at

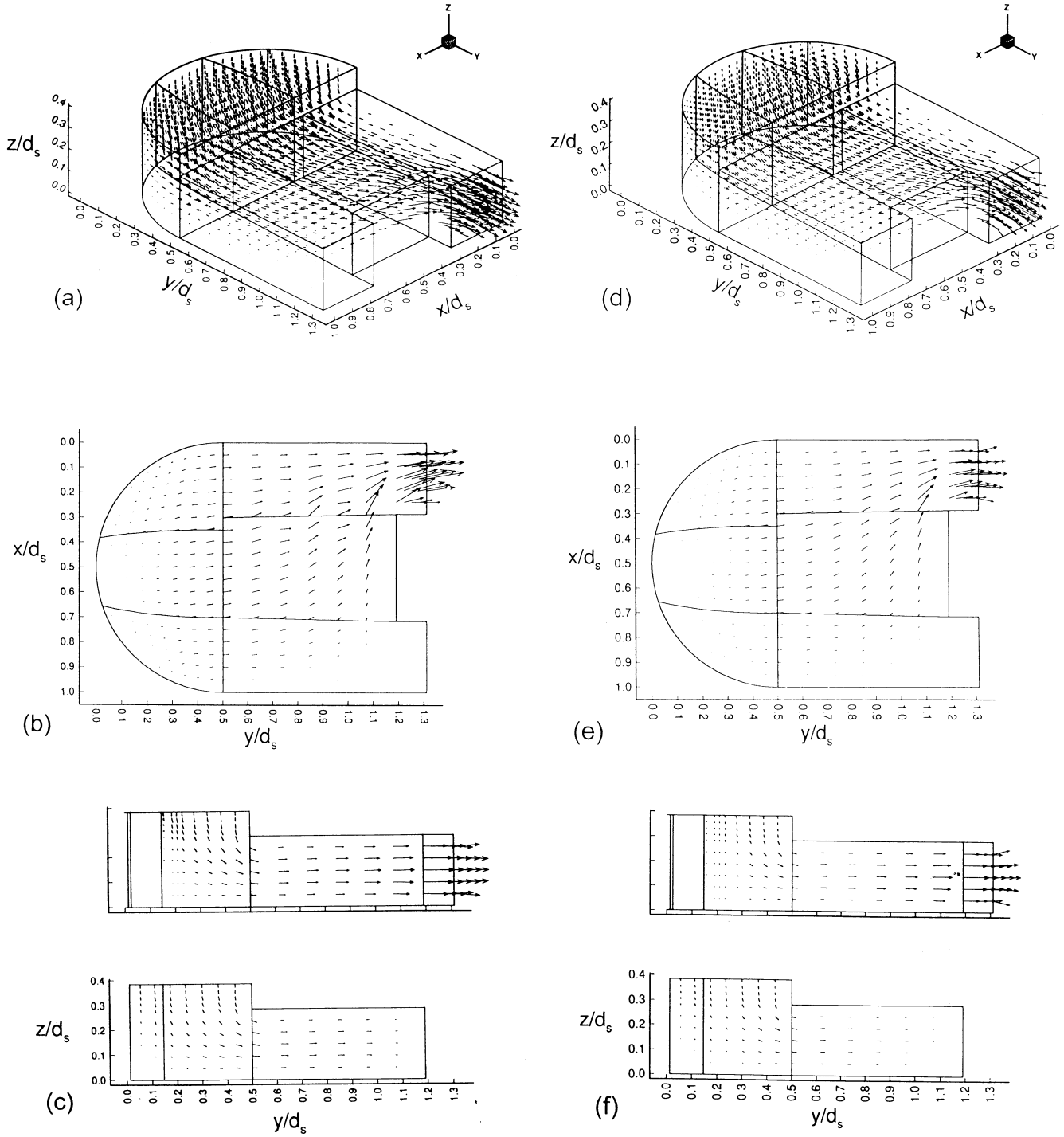

Fig. 3: Velocity vector plots at systolic peak (t/T=0.20), for example 1 (a,b,c) and example 3 (d,e,f): a,d) 3-D views; b,e) cross sections at z/d_s=0.15; and c,f) cross sections at x/d_s = 0.15 (top) and 0.50 (bottom).

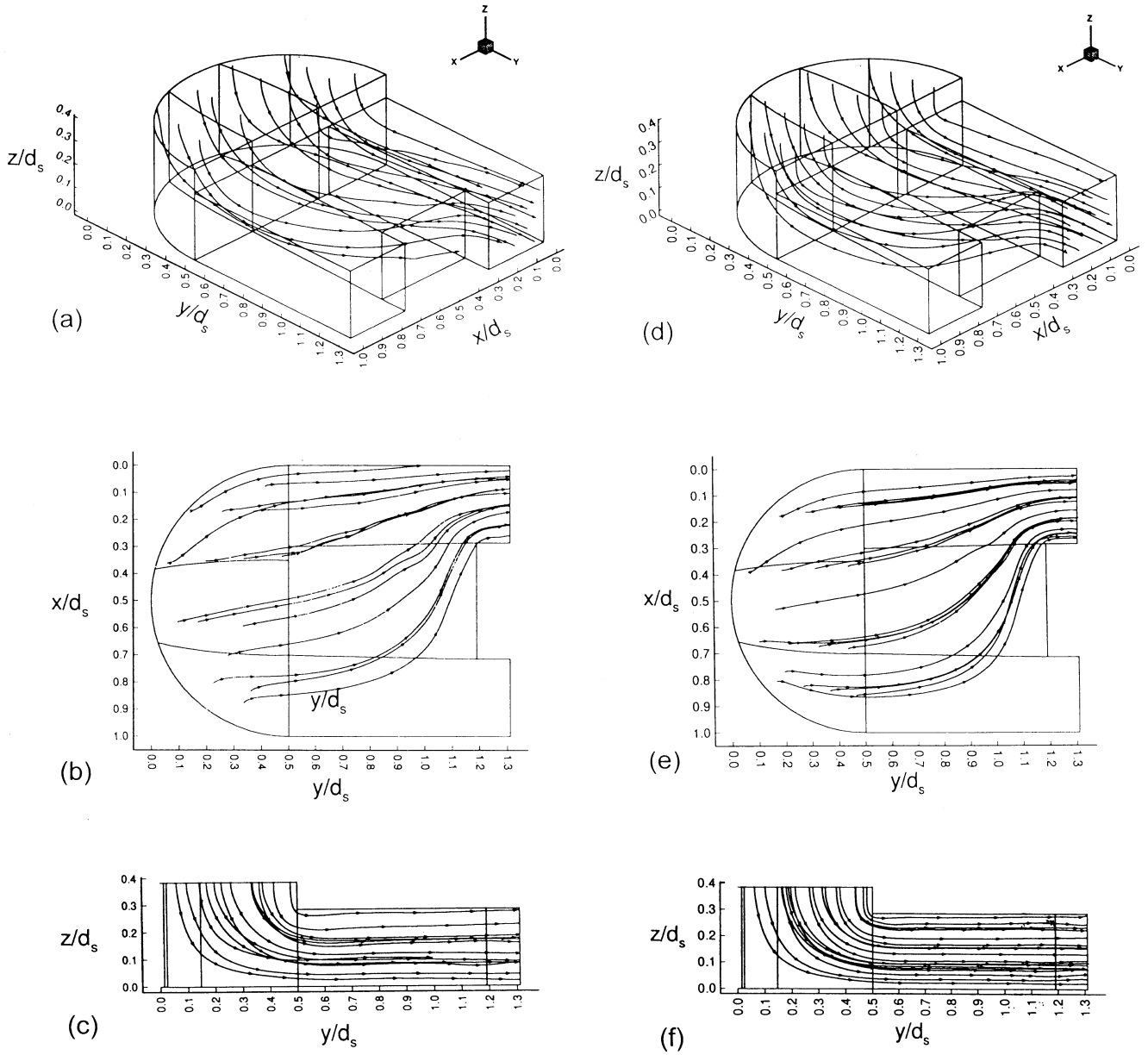

Fig. 4: Streamline plots at systolic peak (*t/T*=0.20), for example 1 (a,b,c) and example 3 (d,e,f): a,d) 3-D views; b,e) top views; and c,f) side views.

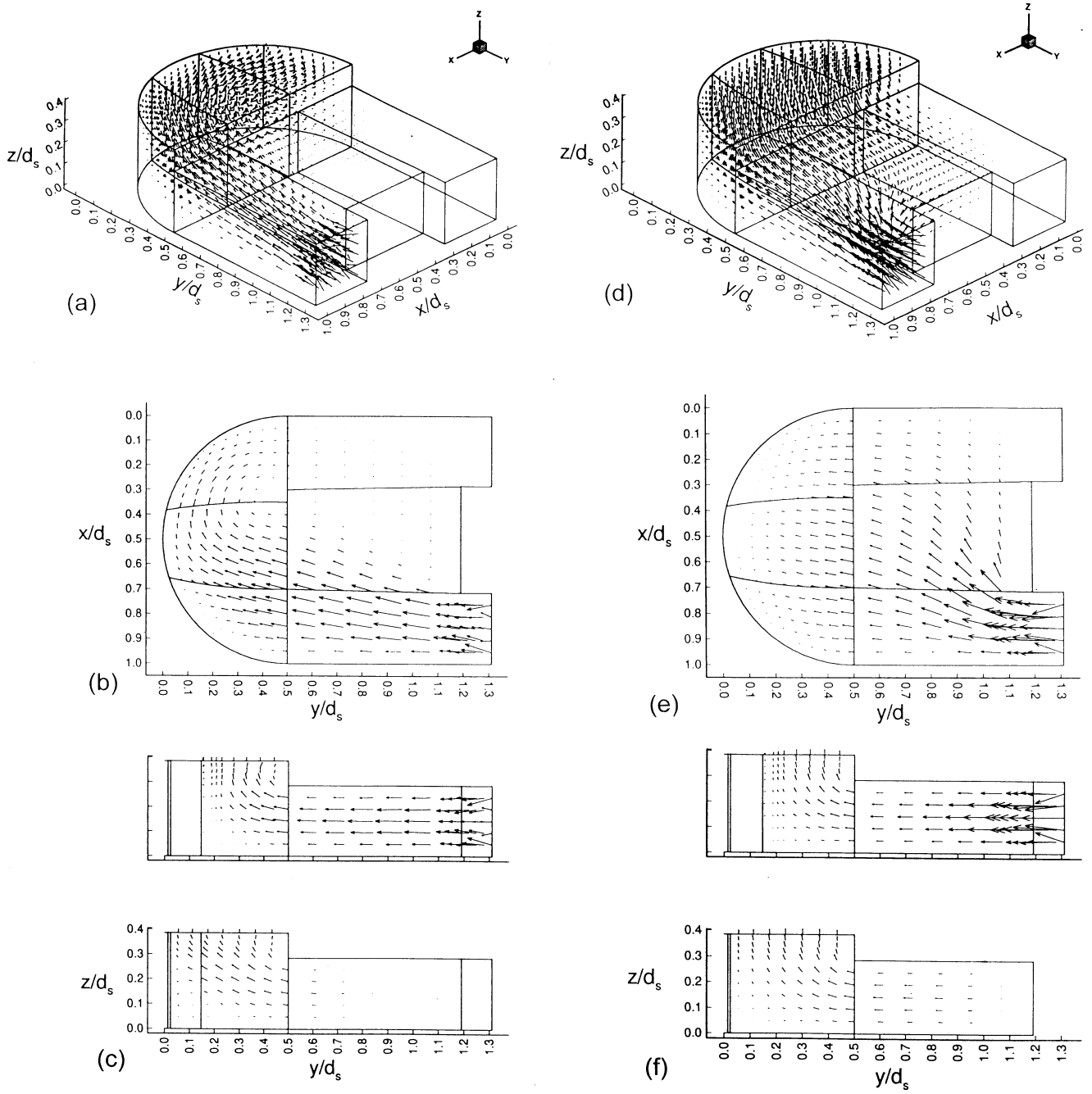

Fig. 5: Velocity vector plots at diastolic peak (t/T=0.76), for example 1 (a,b,c) and example 3 (d,e,f): a) 3-D views; b) cross sections at z/d_s=0.15; and c) cross sections at x/d_s= 0.15 (top) and 0.50 (bottom).

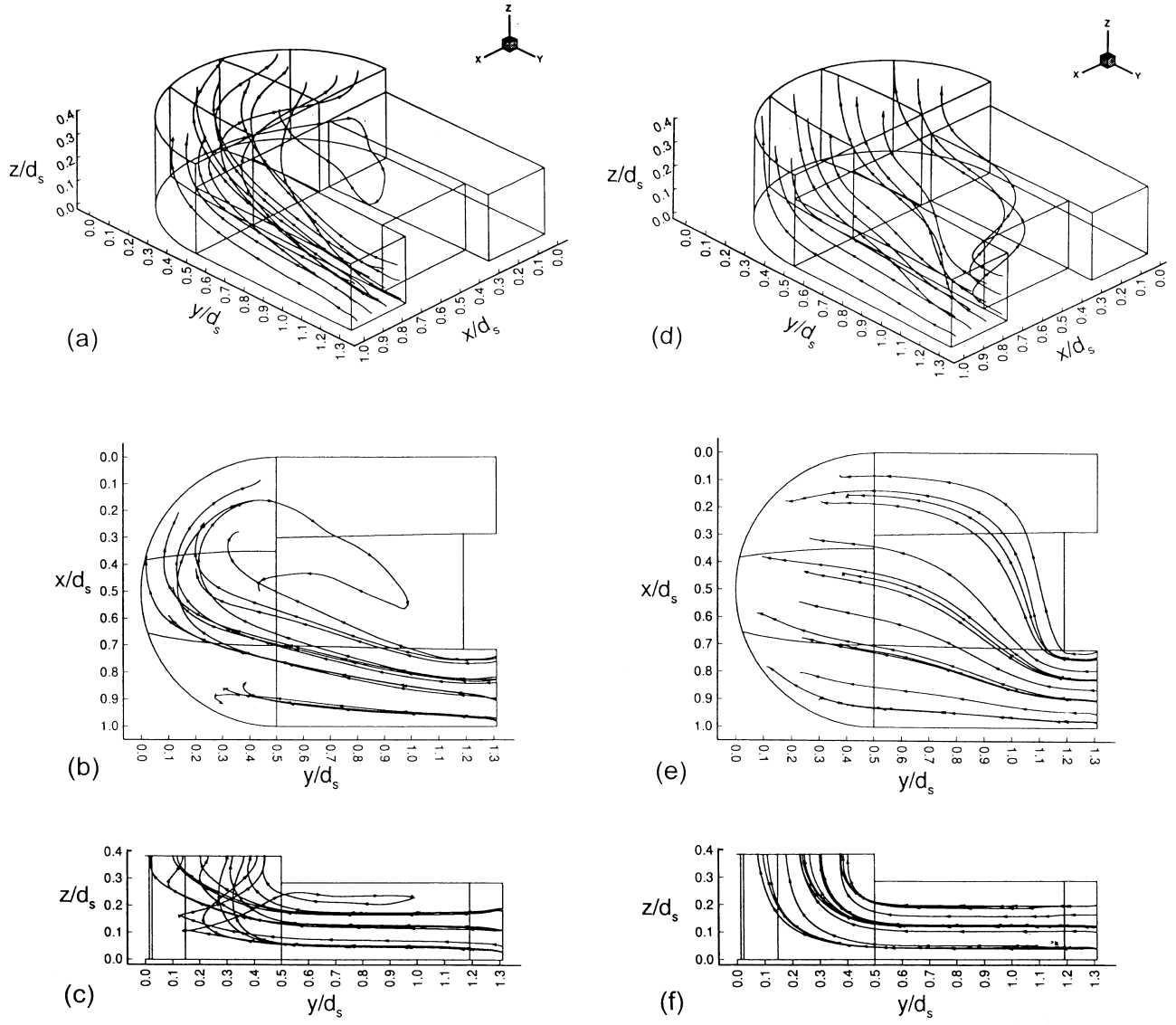

Fig. 6: Streamline plots at diastolic peak (t/T=0.76), for example 1 (a,b,c) and example 3 (d,e,f): a) 3-D views; b) top views; and c) side views.

systolic peak for examples 1 and 3. As the solution converges, the boundary velocity in example 1 (Figure 7a) increases from the zero starting value to the desired value, while remaining uniform across the boundary (except, of course, around the perimeter of Γ_m, where the velocity is forced to be zero). In contrast, the boundary velocity in example 3 (Figure 7b) evolves to a non-uniform distribution, having a maximum located on the side of the open port and diminishing towards the side of the closed port. One may also observe that the velocity profiles near the fixed perimeter tend to be smoother in example 3 than in example 1. In order to diminish the levels of vorticity and stress in the flow, the algorithm generates a skewed optimal boundary velocity variation with higher velocities across open ports and lower velocities across closed ports, while also smoothening the velocity gradient near fixed walls. This strategy could, perhaps, have been foreseen on intuitive grounds. However, the application of optimal control theory is capable of not only manifesting a sound qualitative strategy, but also predicting quantitatively the variation of the control variable that minimizes undesirable effects.

4. Conclusions

In the previous sections we have applied optimal control theory towards the improvement of the hemodynamics of artificial hearts. For the time being, our objective was simply to demonstrate the soundness of this approach. In order to avoid unnecessary complications, we have introduced significant idealizations and simplifications into our model of the heart and the cost functional. Nevertheless, the same procedure could be applied to more realistic models of a given device without any conceptual difficulty, provided that increased computational resources become available. This study has demonstrated that optimal control of flow in artificial organs is feasible and may be used as a design tool.

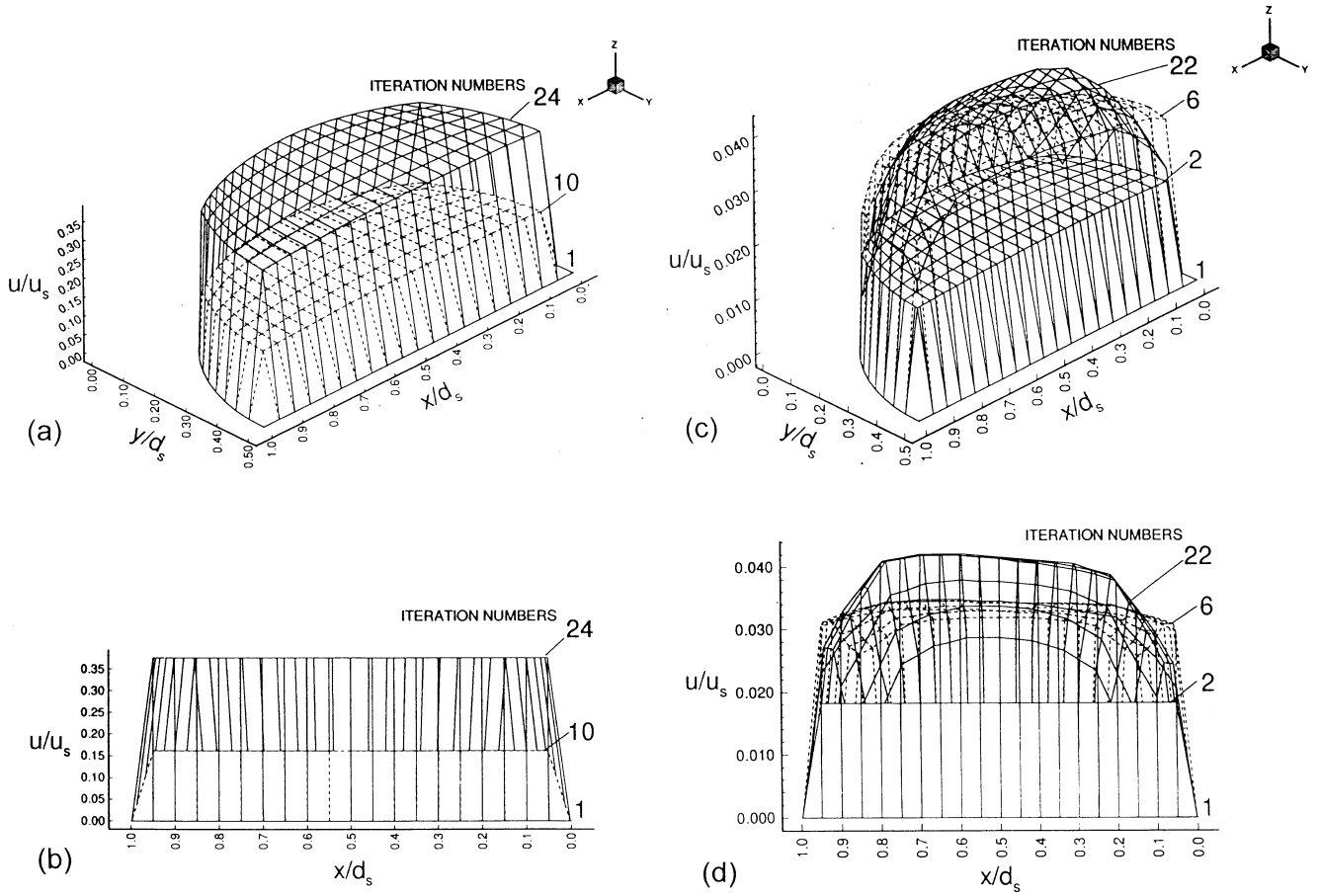

Fig. 7: Evolution of the control boundary velocity at diastolic peak for example 1 (a) and example 3 (b).

Acknowledgement

Financial support for this project was provided in part by the Natural Science and Engineering Research Council of Canada.

References

[1] Abergel F, Temam R (1990) On Some Control Problems in Fluid Mechanics. Theoret Comput Fluid Dynamics 1: 303-325

[2] Ahmed NU (1992) Optimal Control of Hydrodynamic Flow with Possible Application to Artificial Heart. Dynamic Systems and Applications 1: 103-120

[3] Ahmed NU (1995) Mathematical Problems in Modeling Artificial Heart. J Math Problems in Eng 1: 245-254

[4] Blackshear PL, Blackshear GL (1987) Mechanical Hemolysis. In: Skalak R, Chien S (Eds.) Handbook of Bioengineering (pp. 15.1-15.19). New York: McGraw-Hill

[5] Fung Y (1993) Biomechanics: Mechanical Properties of Living Tissues. 2nd ed. New York: Springer-Verlag

[6] Fung Y (1990) Biomechanics: Motion, Flow, Stress and Growth. New York: Springer-Verlag

[7] Galanga F, Lloyd J (1981) An Experimental Study of the Flow-Induced Mass Transfer Distribution in the Vicinity of Prosthetic Heart Valves. J Biomech Eng 103: 1-10

[8] Girault V, Raviart P-A (1986) Finite Element Methods for Navier--Stokes Equations. Berlin: Springer-Verlag

[9] Goldsmith H, Skalak R (1975) Hemodynamics. Ann Rev Fluid Mech 7: 213-247

[10] Gunzburger MD, Hou LS, Svobodny TP (1992) Boundary Velocity Control of Incompressible Flow with an Application to Viscous Drag Reduction. SIAM J Control and Optim 30: 167-181

[11] Hasbani Y, Engelman M (1979) Out-of-Core Solution of Linear Equations with Non-Symmetric Coefficient Matrix. Computers and Fluids 7: 13-31

[12] Jin W, Clark C (1993) Experimental Investigation of Unsteady Flow Behaviour Within a Sac-Type Ventricular Assist Device (VAD). J Biomechanics 26: 697-707

[13] Lesieur M, Métais O (1996) New Trends in Large-Eddy Simulations of Turbulence. Ann Rev Fluid Mech 28: 45-82

[14] Meneveau C, Katz J (2000) Scale-Invariance and Turbulence Models for Large-Eddy Simulation. Ann Rev Fluid Mech 32: 1-32

[15] Mussivand T, Day KD, Naber BC (1999) Fluid Dynamic Optimization of a Ventricular Assist Device Using Particle Image Velocimetry. ASAIO J 45(1): 25-31

[16] Pedley T (1980) The Fluid Mechanics of Large Blood Vessels. Cambridge: Cambridge University Press

[17] Sahrapour A (1995) Optimal Control of Time-Dependent Viscous Flow with Potential Application to Artificial Hearts. Ph.D. Dissertation. Department of Mechanical Engineering, University of Ottawa, Ottawa, Canada

[18] Sahrapour A, Ahmed NU, Tavoularis S (1993) Optimal Control of the Navier--Stokes Equations. In: Proceedings of the First Conference of the CFD Society of Canada, Montreal, pp. 437-448

[19] Sahrapour A, Ahmed NU, Tavoularis S (1994) Boundary Control of the Navier--Stokes Equations with Potential Application to Artificial Hearts. In: Gottlieb J, Ethier C (Eds.) Proceedings of the 2nd Conference of the CFD Society of Canada, Toronto, pp. 387-394

[20] Sritharan SS (Editor) (1998) Optimal Control of Viscous Flow. Philadelphia: SIAM

[21] Stein P, Sabbah H (1974) Measured Turbulence and its Effects Upon Thrombus Formation. Circulation Research 35: 608-614

[22] Tiederman W, Steinle M, Phillips W (1986) Two-Component Laser Velocimeter Measurements Downstream of Heart Valve Prostheses in Pulsatile Flow. J Biomech Eng 108: 59-64